Chinese Chemical Letters 36 (2025) 110510

Contents lists available at ScienceDirect

Chinese Chemical Letters

journal homepage: www.elsevier.com/locate/cclet

Polyvinyl alcohol fiber with enhanced strength and modulus and intense cyan fluorescence based on covalently functionalized graphene quantum dots

Manman Ou, Yunjian Zhu, Jiahao Liu, Zhaoxuan Liu, Jianjun Wang, Jun Sun*, Chuanxiang Qin*, Lixing Dai*

College of Chemistry, Chemical Engineering and Materials Science, Soochow University, Suzhou 215123, China

ARTICLE INFO

Article history:
Received 1 August 2024
Revised 24 September 2024
Accepted 25 September 2024
Available online 26 September 2024

Keywords:
Polyvinyl alcohol fiber
Graphene quantum dots
Enhancement
Fluorescence

ABSTRACT

In this study, we proposed a novel and efficient way to strengthen polyvinyl alcohol (PVA) fiber using graphene quantum dots (GQDs). PVA molecular chains were grafted onto the surface of GQDs through Friedel-Crafts alkylation reaction to obtain functionalized GQDs (f-GQDs), and PVA/f-GQDs composite fiber was successfully prepared by wet spinning and post-treatment. The tensile strength and Young's modulus of the composite fiber reached up to 1229.24 MPa and 35.36 GPa which were approximately twice and 4 times those of the pure PVA fiber, respectively. Moreover, the composite fiber was demonstrated excellent resistance to solvents. In addition, the PVA/f-GQDs composite fiber showed intense and uniform cyan fluorescence, meanwhile, it could maintain stable solid-state fluorescence in acid and alkali solutions and particularly after long-term immersion in water (1 month). This study proposes a promising route for obtaining high-performance conventional fibers with some new functions.

High-performance fiber has become an important strategic material for scientific and technological progress due to its wide range of applications in industry, national defense, aerospace, medical materials, and daily life [1,2]. Compared with the manufacturing of intrinsic high-performance fibers, such as carbon fiber, aromatic fiber, and ultra-high molecular weight polyethylene fiber, the high-performance of regular fiber is more attractive due to its low cost and ease of fabrication. Polyvinyl alcohol (PVA) has great potential to prepare a high-performance fiber because of its similar structure to polyethylene fiber and its high theoretical strength and theoretical modulus [3]. Inspired by the successful preparation of high-strength and high-modulus polyethylene fiber, gel spinning and ultra-drawing have been the main approaches for manufacturing high-performance PVA fiber. However, the improvement in performance is greatly limited by the strong hydrogen bonding between PVA molecular chains, although efforts have been made by many scholars [4-8].

In recent years, due to the excellent mechanical properties of carbon nanomaterials, they have attracted increasing attention as reinforcing agents for polymeric materials. The introduction of one-dimensional carbon nanotubes (CNTs) [5,9-13] and two-dimensional graphene oxide (GO) [4,14-17] to PVA fiber has been a remarkable new way to improve the mechanical properties of the fiber. Most of them are introduced to PVA fiber mainly using physical processes to increase interaction between them, with surface treatment of nanomaterials [4,5,11,12] and the addition of a compatibilizer [9,10,14,15] being common to increase the interaction and dispersity of carbon nanomaterials. However, chemical bonding between carbon nanomaterials and PVA is a more effective method to improve the mechanical properties of PVA fiber, because the covalent functionalization of CNTs can greatly improve the stress transfer from the matrix to CNTs and the dispersity in PVA. For instance, the addition of a small amount of CNTs covalently functionalized with PVA through Friedel-Crafts alkylation reaction leads to a significant increase in the tensile strength of f-MWCNTs/PVA composite fibers [5].

Graphene quantum dots (GQDs) are zero-dimensional carbon nanomaterials [18,19] that are becoming preferred nanofillers for polymers due to their high stability [20], fluorescent properties [21], facile surface functionalization [22], low toxicity [23,24], and environmental friendliness [25,26], and more importantly, they inherit the excellent mechanical strength of graphene. By introducing GQDs into the polymer system, highly stable polymer composites based on GQDs can be prepared with excellent electrical and lumi-

* Corresponding authors.
E-mail addresses: sunjun@suda.edu.cn (J. Sun), qinchuanxiang@suda.edu.cn (C. Qin), dailixing@suda.edu.cn (L. Dai).

https://doi.org/10.1016/j.cclet.2024.110510
1001-8417/

nescent response [27]. The studies regarding GQDs as fillers in PVA matrices have mainly focused on optics [27-32], detection [28,30], sensing [32], memristor [33], and permeation [34], most of which are about their luminescence properties. Compared to CNTs and GO as effective reinforcing agents, GQDs offer some unique merits, higher specific surface area, more abundant active sites, and better dispersibility, thus promoting their interaction and interface compatibility with polymer matrices [19,35,36], so they have the potential to be more suitable as reinforcing agents for the polymer. Currently, research has been conducted on the use of GQDs for the reinforcement of polymers in epoxy resin films [37], polyimide films [38], carbon nanofiber fabrics [39] and silk [40], or the co-reinforcement of polymers with other materials [30,41,42]. However, there are few reports on the use of GQDs for the reinforcement of PVA, one of which is about PVA composite hydrogels formed by the strong hydrogen bonding between GQDs and PVA and between poly(*N*-methylol acrylamide), with the compression fracture stress of the hydrogels twice higher than that of the hydrogels without GQDs [30]. The other few reports only slightly touch upon the enhancement of polymers using GQDs, but the enhancing effectiveness is obviously improved [43]. Apparently, GQDs have the potential to effectively reinforce polymer materials, but thus far, there have been no reports on the application of GQDs in the field of fibers that can most reflect the enhancement effect.

Herein, we proposed an idea for the high-performance PVA fiber by using GQDs as a reinforcing agent for the first time. PVA functionalized GQDs (f-GQDs) were obtained by grafting PVA onto GQDs *via* Friedel-Crafts alkylation reaction, and PVA/f-GQDs composite fiber was prepared by wet-spinning and post-treatment. The composite fiber was endowed with tensile strength of 1229.24 MPa and Young's modulus of 35.36 GPa which were approximately twice and 4 times those of the pure PVA fiber, respectively. Moreover, the composite fiber was demonstrated excellent resistance to solvents. Besides, GQDs endowed PVA fiber with unique fluorescent properties, expanding its use as high-performance PVA fiber and increasing its potential for applications in textile, safety, and environmental protection.

GQDs were prepared by incomplete carbonation of pyrolytic citric acid (CA), forming aromatic and aromatic clusters by aldol condensation and cycloaddition reactions in an easy and nonpolluting process [13]. Fig. 1a shows that the prepared GQDs are well-dispersed spherical particles with relatively uniform sizes, with a particle size distribution ranging from 1.6 nm to 3.0 nm (Fig. S1 in Supporting information). The lattice spacing of 0.37 nm in the HRTEM image (the inset in Fig. 1a) and of 0.35 nm in XRD pattern (Fig. S2 in Supporting information) of GQDs is close to the (002) diffraction plane of graphite [18], indicating the formation of a graphite-like structure.

Fig. 1b shows the FTIR spectrum of GQDs, with a broad and strong absorption band at 3444 cm^{-1} related to the stretching vibrations of -OH and unsaturated C–H bonds [35]. An absorption peak at 1583 cm^{-1} and a shoulder at 1640 cm^{-1} are attributed to the stretching vibrations of C=O in the defect sites of aromatic conjugated alkenes and the skeletal vibrations of C=C conjugation. Combined with the other absorption peaks of the spectrum, such as in-plane bending vibration of -OH at 1396 cm^{-1}, bending vibration of C–O–C at 1230 cm^{-1}, and stretching vibration of C–O at 1080 cm^{-1}, it can be inferred that the prepared GQDs contain abundant oxygen-containing functional groups. The UV–vis absorption and PL spectrum of the obtained GQDs dispersion are shown in Fig. 1c. The UV–vis absorption spectrum shows absorption peaks at 218 nm and 331 nm, which are attributed to π-π^* and n-π^* transitions, respectively [35]. The optimal excitation (Ex) and emission (Em) wavelengths of GQDs dispersion are 366 nm and 450 nm, respectively. Additionally, the inset of Fig. 1c shows that the obtained GQDs dispersion appears nearly colorless under visible light, while it exhibits intense blue fluorescence under 365 nm UV light.

As shown in Fig. 1d, –OH on the PVA molecular chains is deprotonated by the catalytic effect of anhydrous aluminum chloride ($AlCl_3$) and further dissociates to form PVA-C^+. Then, the PVA-C^+

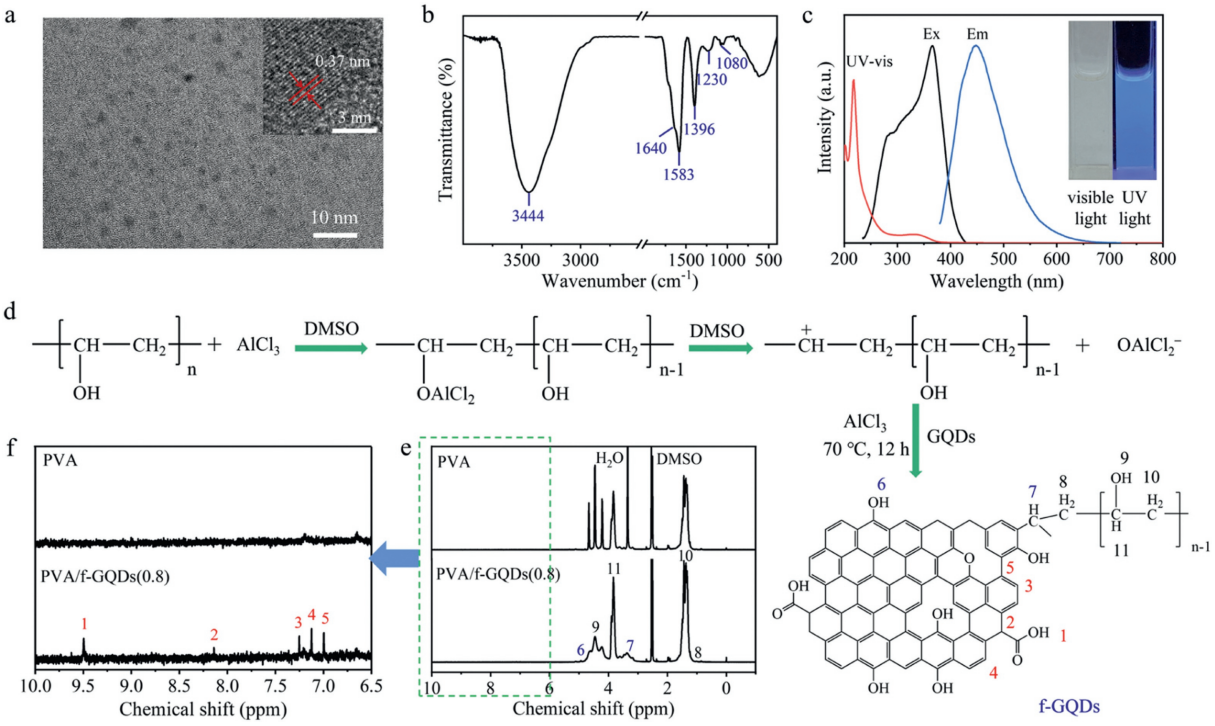

Fig. 1. (a) TEM image of GQDs (inset: HRTEM image of GQDs). (b) FTIR spectrum of GQDs. (c) UV–vis absorption spectrum and PL spectrum of the GQDs dispersion (inset: photographs of the GQDs dispersion under visible light and 365 nm UV light). (d) Schematic diagram of grafting PVA molecular chains to the surface of GQDs by Friedel–Crafts alkylation reaction. (e) ^1H NMR spectra and (f) their local magnification of PVA fiber and PVA/f-GQDs(0.8) composite fiber.

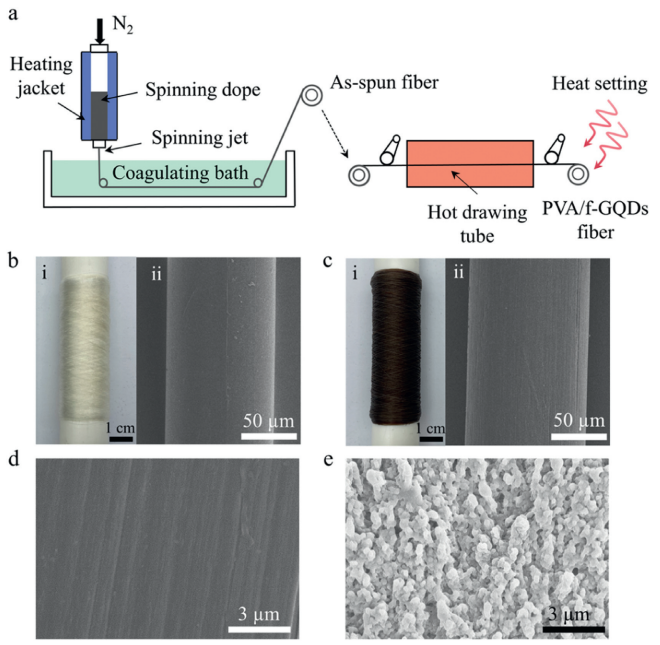

Fig. 2. (a) Diagram for preparation of PVA/f-GQDs composite fiber. Photographs (i) and SEM images (ii) of (b) PVA fiber and (c) PVA/f-GQDs(0.8) composite fiber. (d) Local enlargement of the surface of PVA/f-GQDs(0.8) composite fiber. (e) Cross-section of PVA/f-GQDs(0.8) composite fiber after tension.

electrophilically attacks the active sites on the surface of the GQDs. Subsequently, f-GQDs are prepared by grafting the PVA molecular chains onto the surface of the GQDs through the Friedel–Crafts alkylation reaction.

Figs. 1e and f show the ^{1}H NMR spectra and their corresponding local magnification of PVA fiber and PVA/f-GQDs composite fiber, respectively. In the ^{1}H NMR spectrum of PVA fiber, the peak at 3.3 ppm is attributed to the hydrogen protons of water, while in the spectrum of PVA/f-GQDs(0.8) composite fiber, the peak is significantly weakened. According to the structural formula in the illustration of Fig. 1d, the characteristic peak at 3.3 ppm of hydrogen protons (position 7) corresponds to the connection between the PVA molecular chains and GQDs, which suggests the reason for the weakening of the water peak of the composite fiber. Additionally, the three independent peaks of -OH in the spectrum of the PVA fiber in the range of 4.1–4.7 ppm become a proton triplet peak of the composite fiber, and the intensity of the peak significantly weakened for the composite fiber, which is suggested to be attributed to the change in the chemical environment of -OH due to the chemical bonding between PVA and GQDs. As shown in Fig. 1f, in the ^{1}H NMR spectrum of PVA/f-GQDs composite fiber, distinct proton peaks appear at chemical shifts of 9.4 ppm, 8.1 ppm, 7.2 ppm, 7.1 ppm, and 6.9 ppm, which are characteristic peaks of proton hydrogens on the benzene-like ring (7.0–10.0 ppm) of GQDs. In contrast, neither PVA fiber (Fig. 1f) nor PVA/GQDs blend fiber (Fig. S3 in Supporting information) show peaks in this range, indicating successful covalent bonding between GQDs and PVA molecular chains in the composite fiber.

As shown in Fig. 2a, PVA/f-GQDs composite fiber is prepared by wet spinning and post-treatment including multi-step hot drawing and heat setting. Obviously, the mechanical properties increase with the draw ratio and drawing step (Fig. S4 in Supporting information), and heat setting (Fig. S5 in Supporting information). As shown in Figs. 2b and c, similar to the PVA fiber, the surface of the composite fiber is also smooth and flat, indicating intuitively the uniformity of f-GQDs distribution within the fiber. However, from the enlarged image, it can be observed that the surface of PVA fiber appears still smooth (Fig. S6a in Supporting information), but there are orderly arranged nanoscale grooves along the fiber axis on the surface of the composite fiber (Fig. 2d). GQDs possessing multiple active points not only covalently bonds with PVA chains but also form more hydrogen bonds, which leads to the formation of an interpolymer network. This structure results in an uneven structure, and therefore, one can see that there are many tiny grooves on the surface of the composite fiber [8]. Comparatively, the surface of PVA/GQDs blend fiber is quite smooth, and there are no grooves at all (Fig. S6b in Supporting information), which further proves the stronger interactions between GQDs and PVA molecules.

Ordinarily, the fracture surface of PVA fiber is smooth (Fig. S6c in Supporting information), but the fracture surface of the composite fiber becomes rough with uniformly distributed particles along the tension (Fig. 2e). The particles are formed possibly because f-GQDs can act as regional center points connecting PVA molecular chains in the polymer matrix and can tangle with the surrounding molecular chains, which seems to have some similarity with the literature reports [36,44]. Thus, when subjected to tensile stress, the fiber can effectively transfer loads to GQDs and improve the slip resistance of the macromolecules, thereby increasing the overall strength and modulus.

As shown in Figs. 3a and b, the mechanical properties of the composite fibers exhibit a trend of initial increase followed by a subsequent decrease with increase f-GQDs loadings. It can be noted that when the content of f-GQDs is less than 0.8 wt%, the mechanical properties of the fibers increase gradually to the top value of PVA/f-GQDs(0.8) composite fiber, while when the content is more than 0.8 wt%, the reinforcing effect gradually decreases, which may be related to the aggregation of the particles when an excessive amount is added. At a content of 0.8 wt%, the tensile strength and Young's modulus of the fiber are as high as 1229.24 MPa and 35.36 GPa which are approximately twice and 4 times those of the pure PVA fiber, respectively. In addition, the mechanical properties of the composite fibers are also much greater than those of PVA/GQDs(0.8) blend fiber (Fig. S7 in Supporting information), indicating the better reinforcing effect caused by the covalent bonding of GQDs with PVA. A PVA/f-GQDs(0.8) composite fiber with a diameter of approximately 100 μm is strong enough to repeatedly lift a metal disc weighing 1 kg (Video S1 in Supporting information). Compared to the work reported in the relevant literature on reinforcing PVA fiber with one-dimensional CNTs [5,9,11,12], two-dimensional graphene nanosheets [16,17], cellulose nanocrystals (CNCs) [6,7], cellulose nanofibers (CNFs) [45,46], and others [2,8,47,48], the composite fiber of this work exhibits significant advantages in terms of its mechanical properties (Fig. 3c).

Fig. 3d shows a schematic of the reinforcement mechanism of GQDs on PVA/f-GQDs composite fiber. As stated above, GQDs have more active sites, larger specific surface area, and higher oxygen content than CNTs and GO. On the other hand, in addition to covalent interactions with PVA, the oxygen-containing functional groups on the surface of GQDs, such as hydroxyl and carboxyl groups, can also participate in hydrogen bonding interactions with hydroxyl groups on PVA molecular chains. Therefore, GQDs can act as regional center points connecting PVA molecular chains in the PVA matrix (Fig. 3d, left), which is advantageous for transferring stress from the PVA matrix to GQDs, particularly for the chains covalently bonding with GQDs. The PVA molecular chains connected to the surface of GQDs are helpful to motion transmission between the chains due to the regional center effect of GQDs, so the orientation of the chains is more effective when subjected to tensile stress. In addition, the chains connected to the surface of GQDs are equivalent to increasing the length of PVA molecular chains, which is conducive to the increase of mechanical properties. Meanwhile,

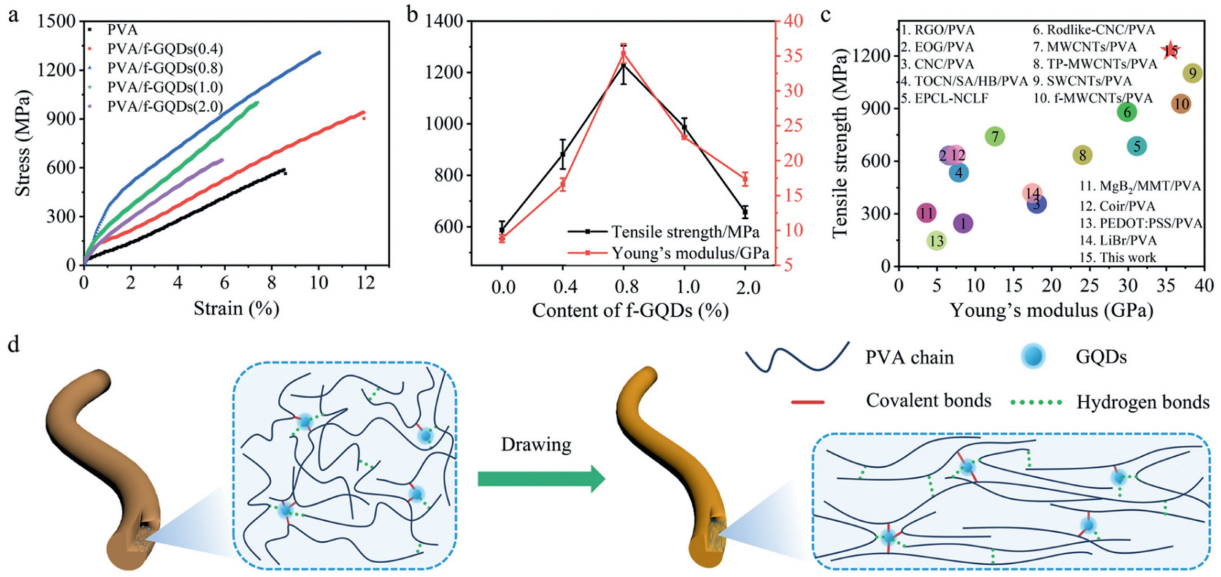

Fig. 3. (a) Stress-strain curves of PVA fiber and PVA/f-GQDs composite fibers with different f-GQDs loadings. (b) Tensile strength and Young's modulus based on the stress-strain curves. (c) Tensile strength and Young's modulus of PVA/f-GQDs(0.8) composite fiber in comparison with those of PVA composite fibers from the literature. (d) Reinforcement mechanism of GQDs on PVA/f-GQDs composite fiber.

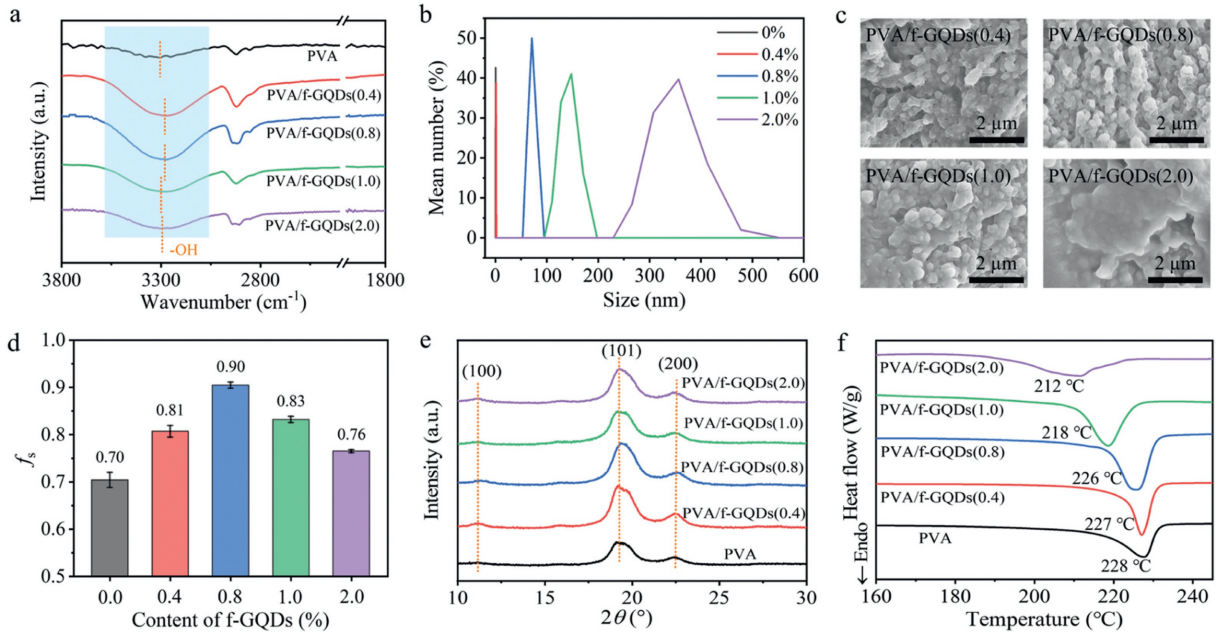

Fig. 4. (a) FTIR spectra of PVA fiber and PVA/f-GQDs composite fibers. (b) DLS size distribution of GQDs in PVA dispersions with different GQDs loadings. (c) SEM of the cross-section of PVA/f-GQDs composite fibers after tension with different f-GQDs loadings. (d) The orientation factor f_s of the composite fibers with different f-GQDs loadings. (e) XRD patterns and (f) DSC curves of PVA fiber and the composite fibers.

improving the interaction between the chains greatly increases the anti-slip ability of the molecular chains (Fig. 3d, right).

As shown in Fig. 4a, when f-GQDs are less than 0.8 wt%, the peak attributed to the hydroxyl group of PVA at 3303 cm^{-1} shifts to a low wavenumber of 3269 cm^{-1} for PVA/f-GQDs(0.8) composite fiber, which suggests an enhancement of hydrogen bonding between GQDs and PVA [4]. However, when the f-GQDs are more than 0.8 wt%, the peak shifts to a slightly higher wavenumber, indicating an increase in the number of free hydroxyl groups, possibly because of the decrease in the number of active sites caused by the aggregation of f-GQDs. Fig. 4b shows that the particle size of GQDs increases with increasing GQDs content in PVA dispersions, particularly when the GQDs content is 2.0 wt%, the size is notably large, and the distribution is broad (240–550 nm), indicating obvious aggregation. When the GQDs content is less than 0.8 wt%, the particle size is less than 100 nm, and the size distribution is narrow, suggesting good particle dispersion and interaction between GQDs and PVA chains. However, as shown in Fig. 4c, different from GQDs in PVA dispersions, f-GQDs in PVA/f-GQDs composite fibers show larger sizes, which is suggested to result from the interaction of many PVA chains with f-GQDs due to the chain orientation during fiber processing. Nevertheless, with f-GQDs loadings higher than 0.8 wt%, aggregation happens, for example at 2.0 wt% block of f-GQDs seems to have formed, which is an important reason for the decrease of the enhancement effect for the composite fibers with the f-GQDs loadings more than 0.8 wt%.

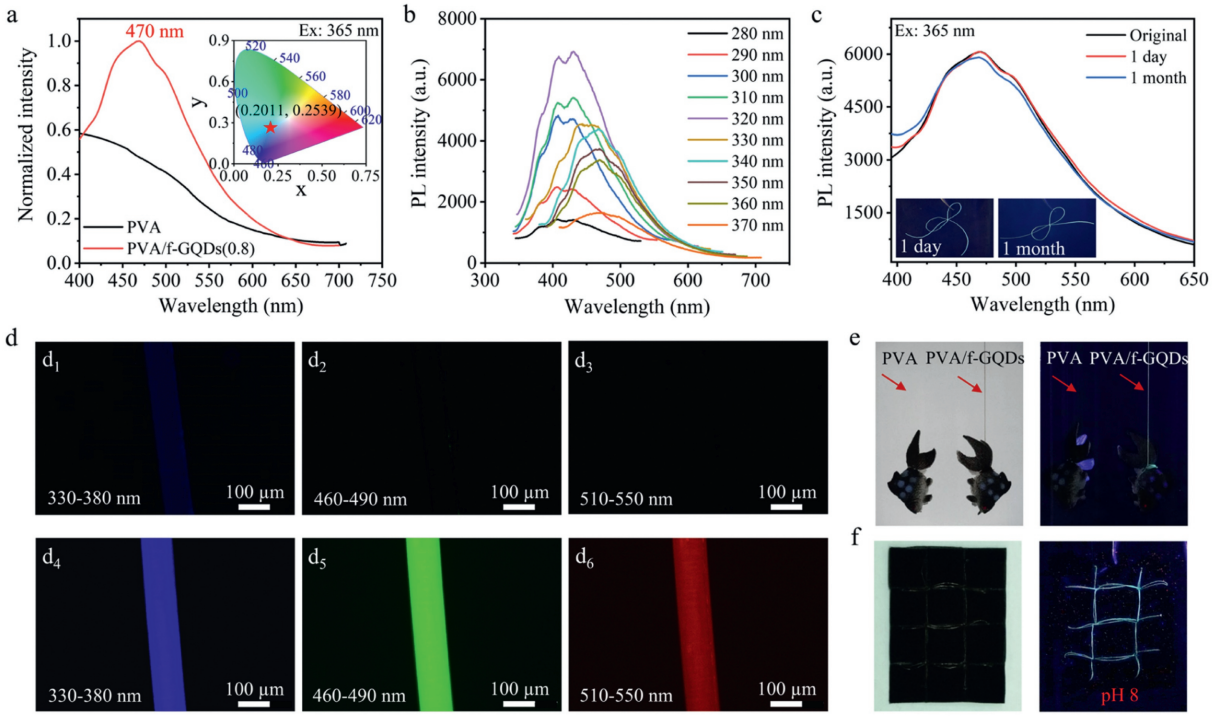

Fig. 5. (a) Fluorescence emission spectra of PVA fiber and PVA/f-GQDs(0.8) composite fiber (inset: CIE 1931 chromaticity diagram of the composite fiber). Fluorescence emission spectra of (b) the composite fiber under different excitation wavelengths and (c) the composite fiber after being soaked in water for different time (inset: photographs of the composite fiber under 365 nm UV light). (d) Fluorescence microscopy images of PVA fiber (d_1–d_3) and the composite fiber (d_4–d_6) under different excitation wavelengths. (e) Photographs of PVA fiber and the composite fiber hanging a loading and immersed in water under visible light (left) and 365 nm UV light (right). (f) Photographs of the composite fiber sewn onto black fabric under visible light (left) and soaked in an alkaline aqueous solution under 365 nm UV light (right).

As shown in Fig. 4d, the orientation of the composite fibers is greater than that of the PVA fiber and shows a first increasing and then decreasing trend with increasing f-GQDs content, which is consistent with the statement that GQDs as regional center points effectively promote the orientation of the molecular chains along the fiber axis. It is worth noting that PVA/f-GQDs(0.8) composite fiber has the highest orientation factor (f_s) of up to 0.90, which is 28% greater than that of the PVA fiber. Fig. 4e shows that the XRD patterns of PVA/f-GQDs composite fibers still maintain the characteristic peaks of the PVA fiber, but the peak intensities of the composite fibers are all greater than those of the PVA fiber. As shown in Table S1 (Supporting information), high peak intensities correspond to high crystallinity and to high mechanical properties. PVA/f-GQDs(0.8) composite fiber also has the highest crystallinity of 52.51%, corresponding to the highest strength and modulus. Similarly, the trend of crystallinities calculated according to the DSC curves is consistent with that calculated based on XRD. By the way, as shown in Fig. 4f, the addition of f-GQDs reduces the melting temperature of PVA fiber, which may be caused by the crosslinking and branching due to the graft of the crosslinker [30]. In conclusion, high crystallinity is related to the high orientation stated above and effective crystallization nucleating agents of f-GQDs in the PVA matrix, while the improved mechanical properties are attributed to the improved crystallinity and orientation due to the introduction of f-GQDs. Moreover, after being exposed to acid, alkali, deionized water, and DMSO for 120 h, the retention rates of the mechanical properties of the composite fiber are maintained at a rate of approximately 85%, demonstrating excellent resistance to solvents (Fig. S8 in Supporting information). Meanwhile, the composite fiber shows good resistance to simulated seawater (Fig. S9 in Supporting information).

Fig. 5a shows the fluorescence emission spectra of PVA fiber and PVA/f-GQDs(0.8) composite fiber. There is no fluorescence emission peak for the PVA fiber under the excitation, that is, the PVA fiber does not emit fluorescence, while the composite fiber exhibits a fluorescence emission peak at 470 nm under an excitation wavelength of 365 nm. Meanwhile, PVA/GQDs(0.8) blend fiber also shows a fluorescence emission peak at 462 nm under the same excitation wavelength (Fig. S10a in Supporting information), indicating the fluorescence properties of PVA fiber endowed by GQDs. A slight red shift of 8 nm is observed for the composite fiber with respect to the blend fiber. This result may be caused by the presence of PVA molecular chains covalently attached to GQDs, which possess extended conjugation (aromatic) structures and hence disrupt the sp^2 network of GQDs and alter the optical properties of GQDs [49]. The inset of Fig. 5a shows that the CIE coordinate of the composite fiber is (0.2092, 0.2539), to which the standard cyan fluorescence (0.1666, 0.2140) is the closest. The excitation-dependent emission spectra recorded for the composite fiber (Fig. 5b) are similar to the corresponding spectra of GQDs in aqueous solution (Fig. S10b in Supporting information), thus confirming that the polymer matrix does not disrupt the fluorescence properties of the added GQDs.

As shown in Fig. 5c, compared to the original, the fluorescence intensity of the composite fiber soaked in water for even 1 month is almost unchanged. After the composite fiber is tied into a butterfly-shaped knot soaked in water for 1 day and then 1 month, under 365 nm UV light, the fiber maintains the shape and intense cyan fluorescence (the inset in Fig. 5c), demonstrating that the composite fiber can maintain stable solid-state fluorescence. As shown in Fig. S11 (Supporting information), the superior hydrophobicity and water resistance of the composite fiber compared to pure PVA fiber is suggested to be one of the main reasons for this.

Fig. 5d shows fluorescence microscopy images of PVA fiber (d_1–d_3) and PVA/f-GQDs(0.8) composite fiber (d_4–d_6). The composite

fiber exhibits stronger blue fluorescence than the PVA fiber under UV excitation (d_1, d_4). When the excitation light is switched to blue and green, the PVA fiber does not fluoresce (d_2, d_3), whereas the composite fiber exhibits intense and uniform green and red fluorescence, respectively (d_5, d_6). Comparatively, PVA/GQDs(0.8) blend fiber only shows dim and uneven fluorescence (Fig. S12 in Supporting information), which infers that covalent bonding of GQDs with PVA chains is helpful to enhance dispersion of the GQDs particles within the PVA matrix, resulting in the superior fluorescence performance of PVA/f-GQDs(0.8) composite fiber.

The excellent mechanical properties and high retention rate in different water environments, and intense fluorescence performance as stated above make the PVA/f-GQDs composite fiber have the potential to be used as fishing nets or threads in water. As shown in Fig. 5e, PVA fiber with a fish-shaped weight hanging in water is almost invisible under both visible and UV light (Fig. 5e, left), while the composite fiber is easily observable under visible light and exhibits intense cyan fluorescence under 365 nm UV light (Fig. 5e, right), making the fiber highly identifiable underwater and facilitating safe operation under nighttime or low visibility conditions. As shown in Fig. 5f and Fig. S13 (Supporting information), the "net-like" pattern of the composite fiber on the fabric is also hard to see under visible light (Fig. 5f, left), but clearly visible under UV light. The "net" is clearly visible under UV light in aqueous conditions at pH 8 (Fig. 5f, right), pH 6 and 7, and the fiber is equally visible in aqueous conditions at pH 4 and 9, indicating stable fluorescence performance in aqueous solutions at different pH.

In this work, we developed an effective strategy for high-performance of PVA fiber with the function of fluorescence for the first time. Covalent interactions between the PVA molecular chains and the surface of GQDs are established in PVA composite fiber through the Friedel-Crafts alkylation reaction, which effectively exerts the reinforcing effect of the GQDs. Moreover, rich active sites on GQDs surface are conducive to forming covalent and hydrogen bonding interactions with PVA molecular chains, leading to improved orientation of the fiber molecular chains. The tensile strength and Young's modulus of the composite fiber reached up to 1229.24 MPa and 35.36 GPa which were approximately twice and 4 times those of the pure PVA fiber, respectively. Moreover, the composite fiber is demonstrated excellent resistance to solvents. In addition, the PVA/f-GQDs composite fiber has intense and uniform cyan fluorescence, meanwhile, it can maintain stable solid-state fluorescence in acid and alkali aqueous solutions and particularly after long-term immersion in water (1 month). This work provides a practical pathway for conventional fibers to achieve high performance along with endowing some functions by introducing appropriate reinforcing agents.

Declaration of competing interest

The authors declare that they have no known competing financial interests or personal relationships that could have appeared to influence the work reported in this paper.

CRediT authorship contribution statement

Manman Ou: Writing – original draft, Validation, Methodology, Investigation, Data curation. **Yunjian Zhu:** Validation, Investigation, Data curation. **Jiahao Liu:** Validation, Investigation, Data curation. **Zhaoxuan Liu:** Validation, Investigation, Data curation. **Jianjun Wang:** Validation, Investigation. **Jun Sun:** Writing – review & editing, Validation, Supervision, Methodology, Investigation, Formal analysis. **Chuanxiang Qin:** Writing – review & editing, Validation, Investigation. **Lixing Dai:** Writing – review & editing, Validation, Supervision, Resources, Methodology, Investigation, Formal analysis, Conceptualization.

Acknowledgments

This research was supported by the National Key Research and Development Program of China (No. 2017YFB0309401), and State and Local Joint Engineering Laboratory for Novel Functional Polymeric Materials of Soochow University.

Supplementary materials

Supplementary material associated with this article can be found, in the online version, at doi:10.1016/j.cclet.2024.110510.

References

[1] C. Gleissner, J. Landsiedel, T. Bechtold, et al., Polym. Rev. 62 (2022) 757–788.
[2] R.A. Saari, R. Maeno, W. Marujiwat, et al., Polymer 213 (2021) 123193.
[3] X. Hong, Y. Xu, L. Zou, et al., J. Appl. Polym. Sci. 138 (2020) e49971.
[4] C. Hu, J. Li, D. Liu, et al., J. Appl. Polym. Sci. 134 (2017) 45463.
[5] P. Zhang, D. Qiu, H. Chen, et al., J. Mater. Chem. A 3 (2015) 1442–1449.
[6] S. Shrestha, F. Montes, G.T. Schueneman, et al., Compos. Sci. Technol. 167 (2018) 482–488.
[7] W.J. Lee, A.J. Clancy, E. Kontturi, et al., ACS Appl. Mater. Interfaces 8 (2016) 31500–31504.
[8] X. Wang, M. Ge, G. Feng, Fibers Polym. 16 (2016) 2578–2585.
[9] L. Lu, W. Hou, J. Sun, et al., J. Mater. Sci. 49 (2014) 3322–3330.
[10] X. Wang, C. Wu, J. Sun, et al., Fibers Polym. 21 (2020) 1078–1085.
[11] D. Lai, Y. Wei, L. Zou, et al., Prog. Nat. Sci. 25 (2015) 445–452.
[12] W.J. Lee, A.J. Clancy, J.C. Fernández-Toribio, et al., Carbon 146 (2019) 162–171.
[13] Y. Dong, J. Shao, C. Chen, et al., Carbon 50 (2012) 4738–4743.
[14] X. Wang, X. Liu, H. Yuan, et al., Mater. Des. 139 (2018) 372–379.
[15] C. Lin, Y. Liu, X. Xie, Chin. Chem. Lett. 30 (2019) 1100–1104.
[16] S. Chen, W. Ma, H. Xiang, et al., J. Power Sources 319 (2016) 271–280.
[17] T. Kim, G. Han, Y. Jung, Materials 12 (2019) 3525.
[18] H. Jia, Y. Cai, J. Lin, et al., Adv. Sci. 5 (2018) 1700887.
[19] Y. Yan, J. Gong, J. Chen, et al., Adv. Mater. 31 (2019) e1808283.
[20] Y. Zhang, S. Lu, Chem 10 (2024) 134–171.
[21] X. Yang, X. Li, B. Wang, et al., Chin. Chem. Lett. 33 (2022) 613–625.
[22] H. Guo, J. Raj, Z. Wang, et al., Small 20 (2024) e2311132.
[23] C. Zheng, S. Tao, Y. Liu, et al., Chin. Chem. Lett. 33 (2022) 4213–4218.
[24] R. Fu, H. Song, X. Liu, et al., Chin. J. Chem. 41 (2023) 1007–1014.
[25] H. Guo, Y. Lu, Z. Lei, et al., Nat. Commun. 15 (2024) 4843.
[26] H. Guo, L. Zhou, W. Hou, et al., Adv. Funct. Mater. 34 (2024) 2402650.
[27] D. Elumalai, B. Rodriguez, G. Kovtun, et al., Nanomaterials 14 (2024) 5.
[28] T. Wang, F. Yang, L. Zhang, et al., Ind. Eng. Chem. Res. 61 (2022) 18090–18099.
[29] B.V.M. Rodrigues, T.S. Cabral, L.F. Sgobbi, et al., Mater. Chem. Phys. 219 (2018) 242–250.
[30] J. Du, W. Zhu, X. She, et al., Polym. Eng. Sci. 63 (2023) 2169–2179.
[31] A. Kovalchuk, K. Huang, C. Xiang, et al., ACS Appl. Mater. Interfaces 7 (2015) 26063–26068.
[32] N.I.M. Fauzi, Y.W. Fen, F.B.K. Eddin, et al., Nanomaterials 12 (2022) 4105.
[33] A. Pisal Deshmukh, K. Patil, K. Barve, et al., Nanotechnology 35 (2024) 265706.
[34] Y. Wan, L. Yao, P. Cui, Chin. J. Chem. Eng. 63 (2023) 226–234.
[35] B. Karimi, B. Ramezanzadeh, J. Colloid Interface Sci. 493 (2017) 62–76.
[36] H. Xu, L. Xie, J. Li, et al., ACS Appl. Mater. Interfaces 9 (2017) 27972–27983.
[37] A. Madhi, B.S. Hadavand, Polym. Plast. Technol. Mater. 61 (2021) 117–130.
[38] Y. Wang, M. Shang, Y. Wang, et al., Fullerenes Nanotub. Carbon Nanostruct. 30 (2021) 683–691.
[39] J. Zhao, J. Zhu, Y. Li, et al., ACS Appl. Mater. Interfaces 12 (2020) 11669–11678.
[40] L. Ma, M.A. Akurugu, V. Andoh, et al., Sci. China Mater. 62 (2018) 245–255.
[41] D. Meng, Y. Hou, D. Kurniawan, et al., ACS Appl. Nano Mater. 7 (2024) 1245–1256.
[42] Y.R. Kumar, K. Deshmukh, M.M.N. Ali, et al., Environ. Res. 203 (2022) 111842.
[43] Q. Sun, L. Zhang, M. Huang, et al., LWT-Food Sci. Technol. 198 (2024) 115953.
[44] C. Min, D. Liu, C. Shen, et al., Tribol. Int. 117 (2018) 217–224.
[45] C. Chen, P. Xi, L. Zhang, et al., Compos. Sci. Technol. 224 (2022) 109464.
[46] P.S. Panicker, D.O. Agumba, J. Kim, ACS Sustain. Chem. Eng. 10 (2022) 10024–10033.
[47] W. Wang, J. He, C. Li, et al., Chem. Eng. J. 462 (2023) 142261.
[48] F. Guo, N. Wang, Q. Cheng, et al., ACS Sustain. Chem. Eng. 4 (2016) 5450–5455.
[49] L. Laysandra, G. Getachew, J. Chang, et al., ACS Appl. Polym. Mater. 5 (2023) 1725–1736.